ACS Energy LETTERS

http://pubs.acs.org/journal/aelccp

LETTER

Vertical Composition Distribution and Crystallinity Regulations Enable High-Performance Polymer Solar Cells with >17% Efficiency

Qingduan Li,[@] Li-Ming Wang,[@] Shengjian Liu,* Lingzhi Guo, Sheng Dong, Guorong Ma, Zhixiong Cao, Xiaozhi Zhan, Xiaodan Gu,* Tao Zhu, Yue-Peng Cai,* and Fei Huang*

Cite This: *ACS Energy Lett.* 2020, 5, 3637−3646

ABSTRACT: The vertical composition distribution and crystallinity of photoactive layers are considered to have critical roles in photovoltaic performance. In this concise contribution, the layer-by-layer (LBL) solution process is used to fabricate efficient polymer solar cells. The results show that the vertical composition distribution can be finely regulated via employing solvent additive 1,8-diiodooctane (DIO). The favorable vertical component distribution in tandem with improved crystallinity induced by DIO contributes to the efficient exciton dissociation, charge transportation and extraction, and limited charge recombination loss. Therefore, the optimized LBL devices yield an efficiency of 16.5%, which is higher than that of the control bulk heterojunction solar cells with an efficiency of 15.8%. Importantly, the ternary solar cells based on PM6/Y6:$PC_{71}BM$ LBL active layers demonstrate a promising efficiency of >17%, which is the record efficiency for LBL solar devices reported to date. These findings make clear that the solvent additive-assisted LBL solution process has broader implications for the further optimization of solar cells.

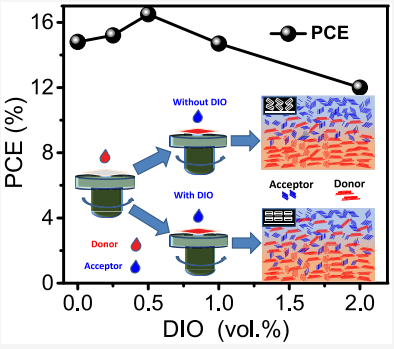

As a potential candidate for renewable energy for future energy sources, polymer solar cells (PSCs) have gained a great deal of attention in recent decades due to their unique advantages, such as their potential for low-cost production via high-throughput roll-to-roll (R2R) processing technology, mechanical flexibility, and light weight.[1−5] The one-step solution process of the blend of electron donors and acceptors that are dissolved in a single solution has been broadly employed to produce a bulk heterojunction (BHJ) photoactive layer, and these types of PSCs are reasonably named BHJ polymer solar cells.[2] Benefiting from combined efforts including novel photovoltaic materials,[6−10] ingenious photoactive layer morphology control,[11,12] and efficient electrode interfacial materials,[3,13,14] the state-of-the-art BHJ PSCs have reached power conversion efficiencies (PCEs) of 16−18% recently.[15−17] Although great success has been obtained in BHJ PSCs,[15,17−19] the one-step solution process technology is not an ideal method for the fabrication of efficient PSCs because (i) the formation of the BHJ morphology is an extremely complicated process,[20−22] (ii) the BHJ morphology of the photovoltaic active layer is strongly dependent on the history of the blend solution,[11,23] (iii) the vertical component distribution is difficult to control precisely,[21,22,24] and (iv) the crystallizations of the donor and acceptor can be disturbed inevitably by each other during the solidification of the blend solution.[25,26] To further realize more efficient and stable polymer solar cells and make this solar technology attractive to industry, the aforementioned issues should be taken into consideration.

Actually, before the invention of BHJ PSCs, the layer-by-layer (LBL) deposition (also named sequential deposition or a two-step process) of the electron donors and electron acceptors was initially used to produce bilayer (also known as planar P−N junction) solar cells in 1986.[27] However, polymer solar cells that were fabricated via the LBL deposition method have met with limited PCEs for a long time due to the well-known limited donor/acceptor interfaces and limited exciton dissociation efficiency in the photoactive layer.[28−30]

Received: September 8, 2020
Accepted: October 21, 2020
Published: October 29, 2020

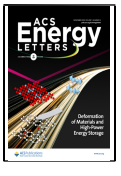

https://dx.doi.org/10.1021/acsenergylett.0c01927
ACS Energy Lett. 2020, 5, 3637−3646

Consequently, the LBL solar device processing method has not attracted attention and has rarely been used to manufacture polymer solar cells in the past three decades. With respect to the vertical component distributions of the photoactive layer, enrichment of the donor near the anode and enrichment of the acceptor near the cathode, which are believed to be favorable for the transportation of charges toward the corresponding electrodes and charge extraction at electrodes, are readily achieved through the LBL device solution process.[20] In addition, the donor and acceptor can maintain the crystallinity of neat films because the donor and acceptor are deposited consequently and independently. Meanwhile, several studies have pointed to the superior stability of LBL polymer solar cells over BHJ solar cells made by the one-step process.[31,32] Hence, the LBL solution process technology is one potential alternative to the one-step solution process technology for producing efficient and stable polymer solar cells.

Historically, orthogonal solvents for dissolving the donor and acceptor are considered to be indispensable for preparing PSCs via the LBL process.[20] Fullerene acceptors (e.g., $PC_{61}BM$, $PC_{71}BM$, and $IC_{71}BA$) possess good solubility (>10 mg/mL) in dichloromethane (DCM) and tetrahydrofuran (THF),[33−35] which usually are poor solvents for polymer donors (e.g., P3HT, PBT7, and its analogues).[36−38] Hence, fullerene-based polymer solar cells could be successfully fabricated through the LBL solution process from polymer donors and fullerene acceptors in their orthogonal solvents sequentially.[39] The LBL PSCs based on P3HT/$PC_{61}BM$,[40] P3HT/$IC_{71}BA$,[41] and PBDTTT-C-T/$PC_{61}BM$[42] reached PCEs of 3.5%, 6.5%, and 7.13%, respectively, which are comparable to that of the control BHJ PSCs made by the one-step solution process. Non-fullerene polymer solar cells, in which small molecule acceptors or polymer acceptors replace the fullerene derivatives, are attracting significant attention in light of their notable photovoltaic performance and stabilities that have been achieved in the conventional one-step-processed BHJ PSCs.[43−46] Recently, those high-performance polymer donors and non-fullerene acceptors have also been used to produce efficient LBL polymer solar cells through spin coating and doctor-blade coating approaches without using orthogonal solvents.[32,47,48]

Solvent additives have been shown to play a key role in the crystallization and grain orientation of donors and acceptors and, thus, have been widely used to optimize the morphology of the BHJ photoactive layer.[49,50] With the most used solvent additive 1,8-diiodooctane (DIO) as an example, DIO was found to be effective in yielding BHJ active layer films featuring a face-on backbone orientation and stronger crystallinity, along with red-shifted ultraviolet− visible (UV−vis) absorption spectra, which are preferable for charge transportation and photon absorption.[18,51] With respect to the LBL solar cells, employing solvent additives to regulate the donor and acceptor interdiffusion and to produce an active layer with the p-i-n structure has rarely been reported.[52] On the basis of the success of solvent additives in controlling the crystallization and grain orientation, it is a key step toward high-performance LBL polymer solar cells to understand how the solvent additive can improve the formation of the p-i-n structure through the LBL solution process.

In this concise contribution, the solvent additive-assisted LBL solution process was used to fabricate efficient polymer solar cells, in which high-performance photovoltaic material polymer donor PM6 and small molecule acceptor Y6 (full names provided in the Supporting Information) were used as the model system. The underlying PM6 donor layer was deposited from its chlorobenzene (CB) solution. The upper Y6 acceptor layer was deposited from its chloroform solution with additive DIO of various volume ratios. The effects of solvent additive DIO on the donor/acceptor interdiffusion and vertical composition distribution of the LBL active layer, along with the crystallinity of photovoltaic materials in thin films, were systematically examined via a combination of neutron reflectivity (NR) and two-dimensional grazing-incidence wide-angle X-ray scattering (2D GIWAXS). The results show that the favorable vertical composition distribution of the LBL active layer, greatly improved crystallinity and backbone "face-on" orientation of Y6, can be simultaneously achieved via tuning the DIO ratios. Upon examination of the devices, the well-regulated p-i-n structure and improved crystallinity in LBL devices processed with DIO were thus translated into efficient exciton dissociation, charge transportation and extraction, and limited charge recombination loss. As a result, the solvent additive DIO (0.5 vol %)-assisted LBL solution process produced high-performance polymer solar cells with a remarkable PCE of 16.5%, which is slightly higher than that of the control BHJ solar cells (15.8%). Moreover, this solvent additive-assisted LBL solution process was further applied to fabricate ternary PSCs to further enhance the photovoltaic performance by taking advantage of its broader light-harvesting and more channels for exciton dissociation. The ternary PSCs, which were deposited from the PM6 donor solution and mixed acceptor (Y6 and $PC_{71}BM$) solution sequentially, reached an even higher PCE of 17.0%, representing one of the highest values that has been obtained for LBL solar devices to date. Most significantly, the PCEs of both binary and ternary LBL solar cells decayed slowly to 15.7% and 16.0%, respectively, while the PCE of the control BHJ solar cells decayed quickly to 13.4% after they had been stored of 1500 h. The superior photovoltaic performance and long-term stability achieved in the LBL solar cells signify the key role of the solvent additive in the regulation of donor and acceptor interdiffusion, crystallinity, and, thus, photovoltaic performance.

Figure 1a provides the chemical structures of polymer donor PM6 and small molecule acceptor Y6. Figure 1b illustrates the

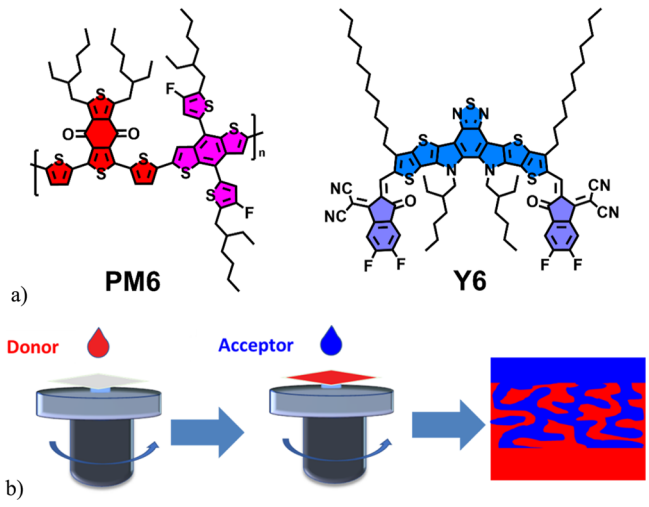

Figure 1. (a) Chemical structure of polymer donor PM6 and acceptor Y6. (b) Illustration of the LBL fabrication method.

https://dx.doi.org/10.1021/acsenergylett.0c01927
ACS Energy Lett. 2020, 5, 3637−3646

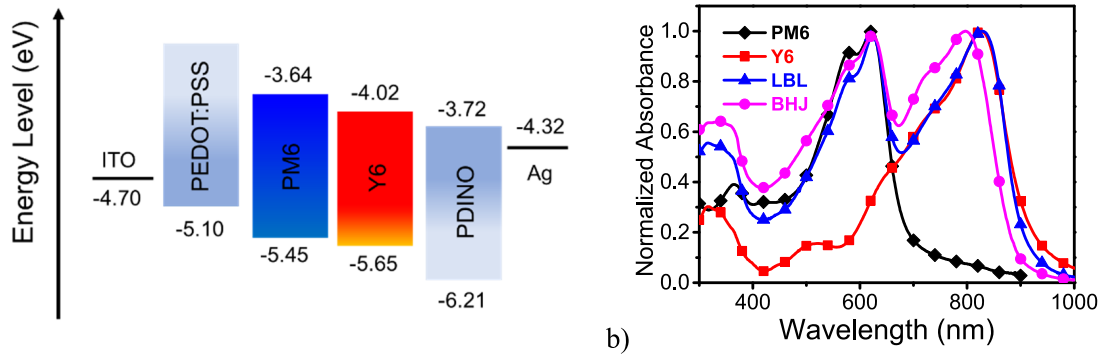

Figure 2. (a) Energy alignment of materials used in this work. (b) Normalized UV−vis absorption spectra of PM6, Y6, LBL PM6/Y6, and BHJ PM6:Y6.

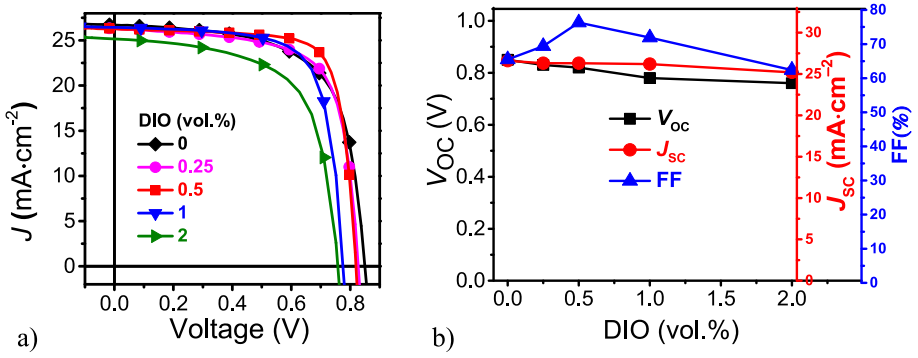

Figure 3. (a) *J*−*V* curves of LBL solar devices processed with different volume ratios of DIO. (b) Figures of merit of LBL solar cells vs DIO volume ratios.

LBL solution deposition method. The LBL photoactive layers were fabricated through spin-coating the two solutions of a neat donor PM6 and a neat acceptor Y6 successively. When casting the chloroform (CF) solution of acceptor Y6, we used 0.25, 0.5, 1, and 2 vol % DIO as the solvent additive to regulate the morphologies of LBL photoactive layers.

The energy alignment of electrodes, photoactive materials, and carrier-transporting materials, which were used in this work, is shown in Figure 2a. Figure 2b emphasizes the complementary absorption spectra of polymer donor PM6 and small molecule acceptor Y6. Generally, the complementary absorption is beneficial for absorbing more photons and producing a higher current. The impact of solvent additive DIO on the light absorption of neat Y6 films was also determined, with the corresponding spectra overlaid in Figure S2a. The absorption peak showed an ∼15 nm red-shift as the DIO ratio increases from 0 to 1 vol %, indicating the formation of more compact aggregation, which is typically promoted by $\pi-\pi$ interactions.

A comparison of light absorption spectra of LBL and BHJ photoactive layers, which are made of the same PM6 and Y6, is provided in Figure 2b. The LBL and BHJ films possess similar light absorption in the range of 400−700 nm that belongs to polymer donor PM6. While in the near-infrared (NIR) range of 700−950 nm that belongs to Y6, the LBL and BHJ films present distinct characteristics. (i) The absorption peak of Y6 in the optimized BHJ film is 797 nm, which is 30 nm blue-shifted compared to that of the neat Y6 film (827 nm). (ii) Y6 in the LBL film possesses the same absorption peak of 827 nm as that of the neat Y6 film. The 30 nm blue-shifted absorption peak of Y6 in the BHJ film, to some extent, suggests that the one-step solution process of the donor/acceptor blend solution would disrupt the crystallization of Y6 during the solidification of the PM6:Y6 in the BHJ film. The unchanged absorption peak of Y6 in the LBL film indicates that Y6 maintains good crystallinity like that of the neat Y6 film, which is helpful for charge generation and transportation in LBL solar cells, representing one of the advantages of the LBL solution-processed solar cells.

As shown in Figure S2b, the absorption spectra of PM6/Y6 LBL films are strongly dependent on the second step solution process parameter, solvent additive DIO. As the DIO ratios increase from 0 to 2 vol %, the PM6/Y6 LBL films showed red-shifted spectra, with corresponding peaks of 817, 822, 827, 830, and 832 nm for LBL films that were processed with 0, 0.25, 0.5, 1, and 2 vol % DIO, respectively. This phenomenon of DIO-induced red-shifted absorption spectra is consistent with prior reports depicting the formation of structural order and $\pi-\pi$ aggregation,[53] which are beneficial for charge transportation (discussed below).

To evaluate the photovoltaic performance of LBL solar cells, thin film devices with the conventional ITO/PEDOT:PSS/PM6/Y6/PDINO/Ag device structure, where the layers of Y6 were cast from a CF solution with various DIO contents (≤2 vol %), were fabricated and examined. The detailed solar device fabrication protocols are provided in the Supporting Information. For a direct comparison, the optimized BHJ solar cells were also fabricated by casting the blend solution of PM6 and Y6 according to a prior report.[54] The *J*−*V* curves of solar cells recorded under simulated AM1.5G sun illumination (100 mW cm^{-2}) are provided in Figure 3a, Figure S3, and Figure S4, with corresponding figures of merit summarized in Table 1 and

https://dx.doi.org/10.1021/acsenergylett.0c01927
ACS Energy Lett. 2020, 5, 3637−3646

Table 1. Photovoltaic Parameters of the LBL Devices Processed with Different Volume Ratios of DIO and Reference BHJ Solar Cells under an Illumination of AM1.5 G, 100 mW cm^{-2}[a]

DIO (vol %)	V_{OC} (V)	FF (%)	J_{SC} (mA cm^{-2})	J_{SC}[b] (mA cm^{-2})	PCE (%) best	PCE (%) average[c]
0	0.85	65.5	26.6	25.8	14.8	14.6
0.25	0.83	69.4	26.3	25.5	15.2	14.9
0.5	0.82	76.3	26.3	25.6	16.5	16.2
1	0.78	71.9	26.2	25.3	14.7	14.3
2	0.76	62.4	25.2	24.6	12.0	11.6
BHJ[d]	0.85	73.5	25.3	24.7	15.8	15.5

[a]Devices were tested under a mask with an area of 0.04 cm^2. [b]The EQE spectra (Figures S4b and S5) integrated J_{SC} values. [c]Averaged performance obtained from >10 devices. [d]Reference BHJ solar cells, optimized devices obtained using previously reported methods.

Table S1. The J_{SC} values obtained from $J-V$ curves (Figure 3a) are coincident with the external quantum efficiency (EQE) spectra (Figure S5) integrated current densities (±0.5 mA cm^{-2}).

As shown in Table 1, the reference BHJ solar cells show a PCE of 15.8%, with a V_{OC} of 0.85 V, a J_{SC} of 25.3 mA cm^{-2}, and a fill factor (FF) of 73.5%, which are comparable to the values reported previously.[54] With respect to the LBL solar cells, the control as-cast (DIO, 0 vol %) device did not manifest any promising performance (PCE = 14.8%), yielding an only modest FF of 65.5% and J_{SC} and V_{OC} values of 26.6 mA cm^{-2} and 0.83 V, respectively. The slight V_{OC} loss of ∼20 meV in LBL devices might be attributed to more substantial nonradiative recombination.[55] However, upon addition of 0.25 and 0.5 vol % DIO in the Y6 solutions, the device FF increases significantly from 65.5% for the as-cast devices to 69.4% and further to 76.3%, indicating that favorable morphological effects are developing in the LBL active layer. Moreover, V_{OC} and J_{SC} remain high (0.82−0.83 V and 26.3 mA cm^{-2}, respectively). Overall, the optimized LBL solar devices processed with 0.5 vol % DIO additive produced significantly enhanced and peak PCEs of ≤16.5%. Here, it is worth noting that PCEs of 16.5% obtained for the optimized LBL cells are greater than PCEs of 15.8% for the optimized BHJ devices, representing one of the promising advantages of LBL solar cells. Upon using more solvent additive DIO, J_{SC}, V_{OC}, and FF decrease concurrently to 25.2 mA cm^{-2}, 0.76 V, and 62.4%, respectively, yielding an inferior efficiency of 12.0% for the LBL devices processed with 2 vol % DIO. As shown in Figure 3b, the DIO additive plays a key role in setting the conditions for high V_{OC}, J_{SC}, FF, and thus PCE values but, in the meanwhile, can be harmful to solar cell operations. Assuming that the DIO directly impacts the migration of the Y6 molecules, a direct examination of the vertical component distribution should reveal significant variations in LBL active layers processed with various levels of DIO.

One of the critical advantages of LBL solution process technology is that the donor-enriched layer near the anode and the acceptor-enriched layer near the cathode, which is essential for efficient charge extraction at electrodes, can be feasibly reached, while the donor/acceptor interface has long been considered to be limited for exciton dissociation. To better determine why these LBL solar cells achieved such superior performance and the pronounced effect of DIO on the LBL device performance, the vertical component distribution of the LBL active layers was examined through neutron reflectometry (NR) measurement, in which the neutron interacts with nucleus. In this work, NR measurements were performed on the multipurpose reflectometer (MR, CSNS, China).[56] The details of the NR experiment and data fitting are provided in the Supporting Information.

The NR reflectivity profiles of neat donor PM6 and neat acceptor Y6 in tandem with their corresponding neutron scattering length densities (SLDs, critical data that can provide the in-depth component concentration of the active layer) are shown in Figure S6. The best fittings for the two reflectivity profiles yield SLDs of 1.005 × 10^{-6} and 2.015 × 10^{-6} Å^{-2} for neat PM6 and neat Y6, respectively. The appropriate SLD contrast ensures the reliable analysis of the vertical component distribution: the volume ratios of PM6 and Y6 versus the in-depth LBL active layer. The SLD of the PEDOT:PSS layer was determined to be 1.53 × 10^{-6} Å^{-2} using the same method, as shown in Figure S6.

With respect to the active layers, the NR data, the fittings, and the corresponding SLD profiles of the LBL thin films processed with different DIO ratios were demonstrated as shown in Figure 4a. A three-layer model was used to determine the vertical component distribution of LBL films without DIO, while a continuously varied SLD model was used to determine the LBL films processed with DIO. All of the simulations give the best fit under their corresponding models, yielding factors

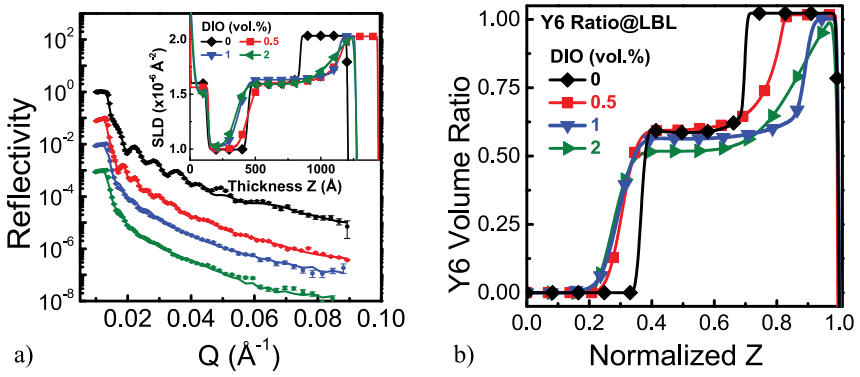

Figure 4. (a) Neutron reflectivity profiles, with reflectivity experimental data shown as individual points and model fits shown as lines, and corresponding models of SLD vs thickness for LBL films without and with DIO. Traces of reflectivity profiles and associated model fits have been offset for the sake of clarity. (b) Y6 volume ratio as a function of normalized thickness profile.

https://dx.doi.org/10.1021/acsenergylett.0c01927
ACS Energy Lett. 2020, 5, 3637−3646

of merit (FOM) of 0.07−0.09 for all LBL films. The sufficiently small FOM ensures that precise information about the LBL films is obtained by the fittings. The vertical component distributions of the LBL films are recorded in SLD profiles shown in the inset of Figure 4a.

The four LBL active layers exhibited two regions with flat Y6 ratios of 0.2 and 99.7 vol % at the bottom and top of the active layers, respectively, suggesting enrichment of donor PM6 at anodes and enrichment of acceptor Y6 at cathodes. Overall, an Y6-enriched layer at the top, a mixed PM6:Y6 layer in the middle, and a pure PM6 layer at the bottom are determined by the NR fitting. The mixed PM6:Y6 layer at the normalized Z axis of 0.4−0.7 is a constituent homogeneous layer due to the interdiffusion effect between the donor and acceptor during the second step solution process, showing a similar pattern of ratio plateau with early LBL-based works.[37] The DIO-induced diffusion of in-depth Y6 molecules among the four LBL samples is strongly exhibited in the transition region between the two layers. As shown in Figure 4a, for the LBL films processed without DIO, the SLD of PM6 abruptly changes to the interdiffusion layer, as does the interdiffusion layer to pure Y6. According to eq S2 in the Supporting Information, the Y6 ratio of the LBL thin film without DIO, indicated as the black line in Figure 4b, shows a relatively sharp change in the transition region from the pure Y6 layer to the mixed constitution layer, which is located at the Z axis of 0.65−0.7, indicating a weaker diffusion of Y6 into PM6 layer compared to those with DIO. On the contrary, in LBL films with 0.5, 1, and 2 vol % DIO show pure Y6 gradually changes to the interdiffusion layer, as do the SLDs. It is worth mentioning that NR also can provide information about the surface roughness of the films. The NR curves of LBL active layers processed without and with optimized 0.5 vol % DIO feature clear Kessing fringes, suggesting the formation of a smooth surface of the two LBL active layers. As the DIO ratio increases to 1 and 2 vol %, the smearing out fringes and quickly dying out tails depend on the Q vector of the NR curves, indicating the rough surface of LBL films. The surface roughness obtained from NR agrees well with the atom force microscopy (AFM) measurement (Figure S7). Overall, a higher level of DIO aggregates PM6 and Y6, forming a coarse interface in both surface and internal films. Moreover, the thickness ratio interdiffusion layer was enhanced among the four samples as the DIO ratio increased. For the "as-cast" LBL active layer, the interdiffusion region maintains a constant ratio, indicating that PM6 and Y6 are distributed homogeneously in the region.[24,50] Among the four LBL films, the "as-cast" LBL film shows the thinnest interdiffusion region. With an increase in the DIO ratios, the interdiffusion region gradually becomes thicker while the donor-enriched and acceptor-enriched layers become thinner (Figure 4b), indicating that larger donor/acceptor interfaces were formed and more Y6 molecules diffused into the underneath PM6 layer with the aid of DIO.

During the spin-coating of Y6 onto the underlying polymer donor PM6 layer, the host solvent chloroform (CF) can swell the donor polymer PM6. Moreover, the Y6 molecules, which were dissolved in CF, can penetrate and diffuse into the PM6 layer in the short duration of solvent volatilization. Consequently, the donor/acceptor interdiffusion layer was formed. Solvent additive DIO, which has a significantly higher boiling point (bp) of 332.5 °C compared to that of CF (only 61.7 °C), will certainly prolong the solvent volatilization and swell more PM6 molecules and, thus, lead to more diffusion of Y6 molecules into the PM6 layer and the formation of a thicker interdiffusion layer. (i) LBL solution process technology can produce a favorable photoactive layer with the p-i-n structure, which is composed of a donor-enriched layer, an acceptor-enriched layer, and a donor/acceptor interdiffusion layer. (ii) Solvent additive DIO showed a pronounced effect in promoting the formation of a donor/acceptor interdiffusion layer and a large donor/acceptor interface, which are beneficial for exciton dissociation. On the basis of the analysis presented above, schematic diagrams of the evolution of the vertical composition distribution in the LBL photoactive layer without and with DIO are provided in Figure 5.

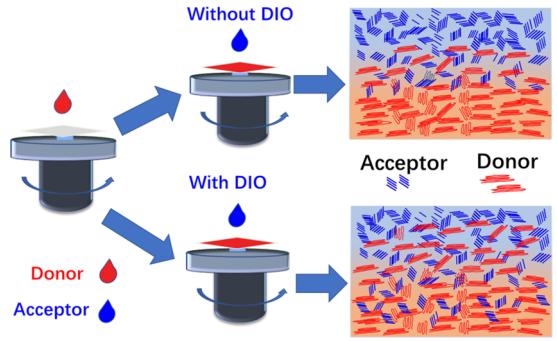

Figure 5. Schematic diagrams of the evolution of the vertical composition distribution in the LBL photoactive layer without and with DIO.

Our NR measurements make clear the presence of larger donor/acceptor interfaces and a thicker interdiffusion region in LBL photoactive layers, which is a critical parameter for exciton dissociation and exciton diffusion. To further examine these characteristics, photoluminescence (PL) quenching analyses and time-resolved PL (TRPL) spectroscopy were performed on those LBL and BHJ photoactive layers. Figures and detailed descriptions are provided in the Supporting Information. The high PL quenching efficiencies shown in Figure S8, to some extent, point out that exciton dissociation in LBL active layers was occurring effectively like that in the optimized BHJ active, which is in good agreement with the presence of large donor/acceptor interfaces in LBL active layers. The TPRL studies, as shown in Figure S9 along with the detailed description in the Supporting Information, also confirmed the efficient exciton dissociation in LBL photoactive layers processed with various DIO volume ratios.

Apart from the vertical component distribution discussed above, self-assembly properties and nanoscale ordering can also be influenced notably by the LBL process parameter, solvent additive DIO. To probe these properties, we examined the LBL and BHJ active layers in a set of 2D GIWAXS. The corresponding GIWAXS patterns are provided in Figure 6 and Figure S10. For the neat Y6 films, clear lamellar ordering and $\pi-\pi$ stacking were observed in the in-plane direction at ≈0.30 $Å^{-1}$ and in the out-of-plane direction at ≈1.75 $Å^{-1}$ (Figure S10b), respectively, indicating that the neat Y6 films adopt a face-on orientation. The enhanced intensity in the in-plane direction at ≈0.30 $Å^{-1}$ and the decreased intensity in the out-of-plane direction at ≈1.75 $Å^{-1}$ were concurrently observed upon processing with DIO additives (Figure S10c), suggesting that DIO can improve the portion of the face-on orientation. Because PM6 and Y6 presented overlaid $\pi-\pi$ and lamellar diffraction peaks, peak summation analysis was performed on

https://dx.doi.org/10.1021/acsenergylett.0c01927
ACS Energy Lett. 2020, 5, 3637−3646

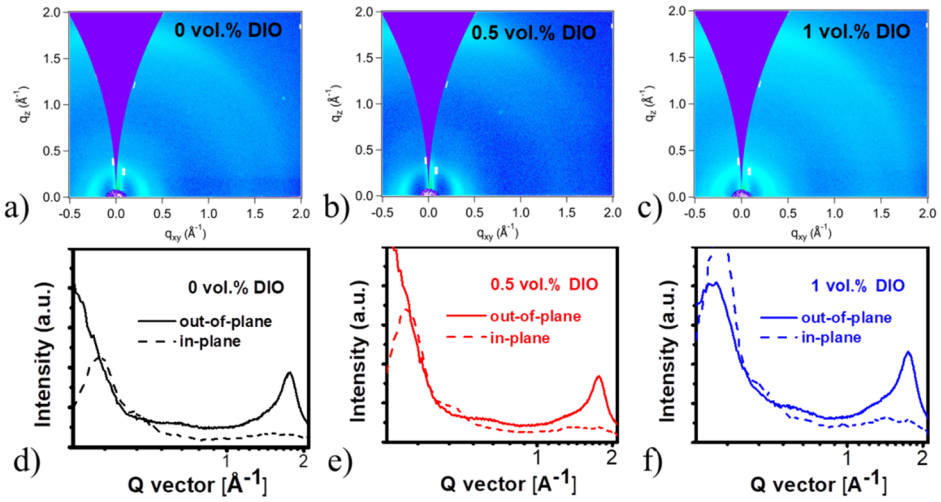

Figure 6. (a–c) 2D GIWAXS patterns and (d–f) in-plane and out-of-plane line cuts of GIWAXS of the LBL active layers with various DIO contents: (a and d) 0 vol % DIO, (b and e) 0.5 vol % DIO, and (c and f) 1 vol % DIO.

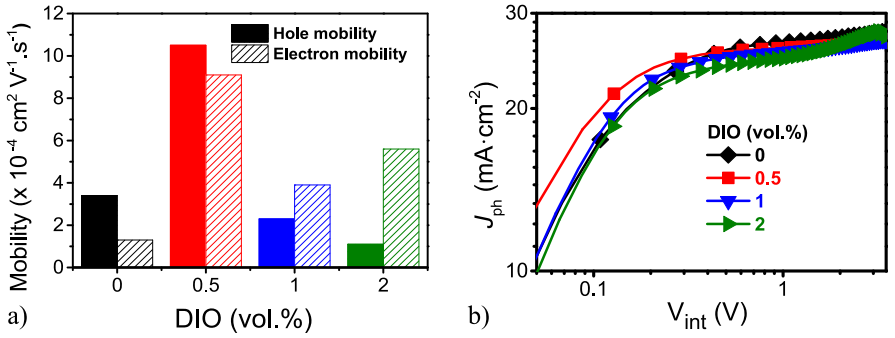

Figure 7. (a) Histogram of hole and electron mobilities determined by SCLC measurements. The solidly colored bars show data for hole-only devices. The patterned line bars show data for electron-only devices. (b) Photocurrent density (J_{ph}) vs internal voltage (V_{int}) for LBL devices.

the LBL and BHJ films. As summarized in Tables S2 and S3, detailed peak fittings of out-of-plane profiles showed that LBL films with 0.5 vol % DIO presented improved crystallinity compared to that of LBL films without DIO. The crystal size of the domains could be estimated by the calculated crystal coherence (CCL, CCL = $2\pi k$/fwhm),[58] in which k is the shape factor typically defined as 0.9 and fwhm is the half-width of the diffraction peak. The lengths (CCL) are summarized in Table S4. The LBL film processed with 0.5 vol % DIO showed a CCL of 25.21 Å, which is larger than that of the "as-cast" LBL film (19.22 Å). A high CCL points to the improved crystallinity, which is often favorable for charge transport, whereas as the DIO ratios further increase to 1 vol %, the CCL decreased to 23.25 Å, indicating the lower crystallinity. As we conclude from Figures S2 and S10, it seems that the crystallinity of neat Y6 films improves as the DIO ratio increases. When Y6 was solution-coated atop the PM6 layer, the NR examination (Figure 4b) makes clear that solvent additive DIO would promote the diffusion of more Y6 molecules into the PM6 layer. The crystallization kinetics of Y6, which diffused into the PM6 layer, can be disturbed by the donor materials. Thus, the diffusion of Y6 molecules can explain why the LBL active layer processed with 1 vol % DIO showed a crystallinity slightly lower than that of the optimized LBL active layer (0.5 vol % DIO). Overall, these results suggest that the solvent additive-assisted LBL solution process technology can improve the crystalline quality of the active layers, which can be beneficial for charge transport and elucidate the improved FF for LBL solar devices.

Given the marked changes in the donor/acceptor interface, the vertical component distribution and molecular packing occurring in LBL active layers, charge transport, recombination, and extraction may differ, consequently impacting photovoltaic performance. Therefore, the space charge-limited current (SCLC) measurements (see the experimental details in the Supporting Information) were used to determine the hole and electron mobilities. Figure S11 and Table S5 present the $J^{1/2}$–V fitting results and the calculated mobilities, respectively. For easy comparison, the charge mobilities are plotted in a histogram as shown in Figure 7a. Devices processed with various levels of DIO achieved very distinct charge mobilities. However, the "as-cast" LBL device (0 vol % DIO) exhibited rather modest hole and electron mobilities of 3.4×10^{-4} and 1.3×10^{-4} cm^2 V^{-1} s^{-1}, respectively. It is worth noting that the "as-cast" LBL active layer possesses a limited interdiffusion region and thick donor and acceptor-enriched layers (Figure 4b), meaning the lack of a continuous charge transport network. When the LBL active layer is processed with 0.5 vol % DIO, a more continuous charge transport network and better crystalline quality (Figure 6b) are concurrently formed. Hence, hole and electron mobilities improved significantly to peak values of 1.1×10^{-3} and 9.1×10^{-4} cm^2 V^{-1} s^{-1},

https://dx.doi.org/10.1021/acsenergylett.0c01927
ACS Energy Lett. 2020, 5, 3637–3646

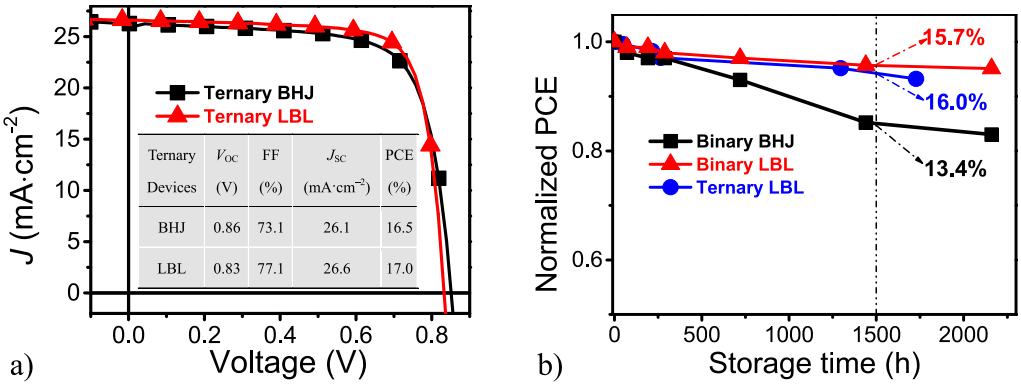

Ternary Devices	V_{OC} (V)	FF (%)	J_{SC} (mA·cm^{-2})	PCE (%)
BHJ	0.86	73.1	26.1	16.5
LBL	0.83	77.1	26.6	17.0

Figure 8. (a) *J*–*V* curves of the optimized ternary LBL and BHJ solar devices, ITO/PEDOT:PSS/active_layer/PDINO/Ag. Detailed information about the active layer is provided in the Supporting Information. (b) Stability tests of LBL and BHJ solar devices stored in a nitrogen atmosphere.

respectively, which are 3 and 8 times higher than that in the "as-cast" devices, respectively. Generally, the higher carrier mobilities benefit the FF and lead to an overall highest PCE value of 16.5% in devices. As the DIO ratio further increases, hole and electron mobilities decrease dramatically, which could be attributed to the lower crystallinity as determined by the GIWAXS examination. Interestingly, a zigzag tendency of electron mobility with an increasing DIO volume ratio was observed, which is attributed to the trade-off between the crystallinity and the continuity of the Y6 component across the LBL thin film. To be specific, as the DIO volume ratio further increased to 2 vol %, the crystallinity of Y6 is almost the same as that with 1 vol %, but the continuity of Y6 in the overall film is better. As indicated in Figure 4b, the LBL film exhibits a better gradient vertical distribution over the *Z* axis of 0.7–1, which could be beneficial for electron transport.

With respect to the exciton dissociation and charge collection losses, the evolution of the photocurrent density (J_{ph}) with internal voltage (V_{int}) for LBL devices and the dependence of V_{OC} and J_{SC} on incident light intensity (I) were examined. As illustrated in Figure 7b, the J_{ph} for the optimized LBL device (0.5 vol % DIO) increases quickly when V_{int} < 0.1 V and reaches a saturation regime early when V_{int} > 0.3 V. As for other devices, the J_{ph} shows slightly field-dependent behavior, which is indicative of inefficient charge extraction. Moreover, the exciton dissociation and charge collection efficiency, with calculation details provided in the Supporting Information, were measured under the short circuit condition and maximum power output point, respectively. As concluded in Table S6, the optimized LBL devices (0.5 vol % DIO) presented significantly improved and highest η_{diss} and η_{coll} values of 98.5% and 84.2%, respectively, indicating efficient exciton dissociation and charge collection, which agree well with the aforementioned favorable donor/acceptor interfaces, vertical component distribution, molecular packing, and the peak FF value of 76.3%. Figure S12a plots the variation of J_{SC} as a function of I on a log–log scale, fitting to a power law $J_{SC} \propto I^{\alpha}$ (solid lines). As shown in Figure 12a, all of the devices showed similar exponential factor a values of 0.97–0.99, which are approaching unity. The high α values of 0.97–0.99 reflect weak bimolecular recombination losses under short circuit conditions. In other words, the free carriers are extracted efficiently by the electrodes as a result of the desirable vertical component distributions that are formed in LBL active layers. With respect to another loss mechanism, trap-assisted charge recombination, Figure S12b plots the dependence of V_{OC} as a function of I on a log-linear scale, fitting to the equation $V_{OC} \propto n\frac{kT}{q}\ln(I)$. k, T, and q are the Boltzmann constant, temperature in kelvin, and elementary charge, respectively. As shown in Figure S12b, the optimized LBL device (0.5 vol %) showed a lowest n value of 1.10, which is close to unity (trap-free condition) and reflects the negligible trap-assisted recombination across the active layer or at electrodes. On the contrary, large n values of 1.31–1.38 were inferred for other LBL solar devices, indicating that trap-assisted recombination is serious under the open circuit condition.

As concluded from the aforementioned systematic studies, LBL deposition can easily produce a favorable vertical component distribution, with the donor-enriched layer near the anode and the acceptor-enriched layer near the cathode. This type of vertical component distribution is essential for negligible charge recombination loss across the active layers and efficient charge extraction at electrodes. Thus, the LBL deposition technology was further extended to fabricate ternary solar cells, which could provide additional means for further enhancing photovoltaic performance, spaning (i) complementary light absorption, (ii) improved charge transfer (exciton dissociation) through the cascade energy level, (iii) energy transfer between components, and (iv) optimized morphology. According to the procedure for the aforementioned binary LBL devices, various weight ratios of $PC_{71}BM$ were added as the second acceptor during the solution processing of Y6. The general experimental details are provided in the Supporting Information. On the basis of the prior NR analysis of the binary LBL active layers, there is no doubt that the Y6 and $PC_{71}BM$ small molecules could diffuse into the underlying PM6 layer, and thus, donor-enriched, acceptor-enriched, and interdiffusion layers are formed in ternary LBL solar devices. The *J*–*V* and EQE curves of the champion ternary LBL solar devices, in which the optimized Y6:$PC_{71}BM$ ratio is 1.0:0.2, are provided in Figure 8a and Figure S13, respectively. The ternary LBL solar device produced a significantly improved FF of 77.1% and gentle J_{SC} and V_{OC} values of 26.6 mA cm^{-2} and 0.83 V, respectively. Overall, the device reached a PCE of 17.0%, representing one of the highest values obtained for LBL solar devices to date.[48,59] The ternary BHJ solar cells, which are composed of the same photovoltaic materials, PM6, Y6, and $PC_{71}BM$, were also fabricated for comparison. As shown in Figure 8a, the optimized ternary BHJ solar cells exhibited an FF of 73.1%, a

https://dx.doi.org/10.1021/acsenergylett.0c01927
ACS Energy Lett. 2020, 5, 3637–3646

J_{SC} of 26.1 mA cm^{-2}, a V_{OC} of 0.86 V, and an overall PCE of 16.4%, which is slightly lower than that obtained in ternary LBL solar cells. The overall PCE histograms of optimized ternary BHJ and LBL solar cells are summarized in Figure S14. The superior photovoltaic performance achieved in ternary LBL solar devices also highlights the significant potential of LBL solution technology in fabricating efficient polymer solar cells.

Besides photovoltaic performance, we compare another practical property, device stability. The evolution of photovoltaic PCEs versus storage time was examined and is shown in Figure 8b. As provided in Figure 8b, the control BHJ solar devices showed poor stability. The BHJ solar devices presented a significantly decreased PCE of 13.4%, which preserved <80% of its original PCE value after storage for 1500 h. In contrast, the PCEs of both binary and ternary LBL solar cells decayed to only 15.7% and 16.0%, respectively, which preserved >95% of its original PCEs. All in all, the data shown in Figure 8b signify the superiority of LBL solar cells over BHJ solar cells in device storage stability, representing an additional advantage of the LBL solution technology.

In summary, we showed that LBL solution process technology (also known as sequential deposition or the two-step solution process) can produce efficient solar cells, reaching PCE values of 16.5% and 17.0% in binary and ternary LBL solar cells, respectively. Our systematic solar cell optimizations show that the LBL solution process parameter, solvent additive DIO, showed a significant effect on the photovoltaic properties. In particular, solar cell FFs increase markedly from ≈65% for "as-cast" devices to ≈77% for the optimized devices processed with 0.5 vol % DIO. Detailed examinations of the NR measurements make clear that larger donor/acceptor interfaces, a thicker interdiffusion region, a donor-enriched layer near anodes, and an acceptor-enriched layer near cathodes can be concurrently reached in LBL active layers with the aid of solvent additive DIO. 2D GIWAXS analyses showed the DIO can improve the crystallinity and backbone "face-on" orientation in the optimized LBL actives (0.5 vol %). The superior photovoltaic performance and long-term device stability of LBL solar cells over BHJ solar cells signify that LBL solution process technology is a potential candidate for device fabrication for producing more efficient polymer solar cells. Our contribution further emphasizes the vital importance of tailoring the interdiffusion layer (vertical component distribution) in the efficiency enhancement of LBL solar cells.

■ ASSOCIATED CONTENT

Supporting Information

The Supporting Information is available free of charge at https://pubs.acs.org/doi/10.1021/acsenergylett.0c01927.

Details of device fabrication and polymer solar cell characterization; charge carrier mobility measurements; PL quenching analyses and TRPL spectroscopy; NR and 2D GIWAXS measurements; AFM data; and additional figures and tables (PDF)

■ AUTHOR INFORMATION

Corresponding Authors

Shengjian Liu − *School of Chemistry, Guangzhou Key Laboratory of Materials for Energy Conversion and Storage, South China Normal University (SCNU), Guangzhou 510006, China;* orcid.org/0000-0001-8492-3176; Email: shengjian.liu@m.scnu.edu.cn

Xiaodan Gu − *School of Polymer Science and Engineering, Center for Optoelectronic Materials and Devices, The University of Southern Mississippi, Hattiesburg, Mississippi 39406, United States;* orcid.org/0000-0002-1123-3673; Email: xiaodan.gu@usm.edu

Yue-Peng Cai − *School of Chemistry, Guangzhou Key Laboratory of Materials for Energy Conversion and Storage, South China Normal University (SCNU), Guangzhou 510006, China*; Email: caiyp@scnu.edu.cn

Fei Huang − *Institute of Polymer Optoelectronic Materials and Devices, State Key Laboratory of Luminescent Materials and Devices, South China University of Technology (SCUT), Guangzhou 510640, P. R. China;* orcid.org/0000-0001-9665-6642; Email: msfhuang@scut.edu.cn

Authors

Qingduan Li − *School of Chemistry, Guangzhou Key Laboratory of Materials for Energy Conversion and Storage, South China Normal University (SCNU), Guangzhou 510006, China;* orcid.org/0000-0002-0641-5798

Li-Ming Wang − *Spallation Neutron Source Science Center, Dongguan 523803, China; Institute of High Energy Physics, Chinese Academy of Sciences, Beijing 100049, China*

Lingzhi Guo − *School of Chemistry, Guangzhou Key Laboratory of Materials for Energy Conversion and Storage, South China Normal University (SCNU), Guangzhou 510006, China*

Sheng Dong − *Institute of Polymer Optoelectronic Materials and Devices, State Key Laboratory of Luminescent Materials and Devices, South China University of Technology (SCUT), Guangzhou 510640, P. R. China*

Guorong Ma − *School of Polymer Science and Engineering, Center for Optoelectronic Materials and Devices, The University of Southern Mississippi, Hattiesburg, Mississippi 39406, United States*

Zhixiong Cao − *School of Chemistry, Guangzhou Key Laboratory of Materials for Energy Conversion and Storage, South China Normal University (SCNU), Guangzhou 510006, China*

Xiaozhi Zhan − *Spallation Neutron Source Science Center, Dongguan 523803, China; Institute of High Energy Physics, Chinese Academy of Sciences, Beijing 100049, China*

Tao Zhu − *Beijing National Laboratory for Condensed Matter Physics and Institute of Physics, Chinese Academy of Sciences, Beijing 100190, China*

Complete contact information is available at: https://pubs.acs.org/10.1021/acsenergylett.0c01927

Author Contributions

[@]Q.L. and L.-M.W. contributed equally to this work.

Notes

The authors declare no competing financial interest.

■ ACKNOWLEDGMENTS

This work was financially supported by the National Natural Science Foundation of China (21805097, 21671071, and 51521002), the Guangdong Natural Science Foundation (2019A1515012137), the Guangdong Applied Science and Technology Planning Project (2015B010135009 and 2017B090917002), the Guangzhou Science and Technology Foundation (201904010361), and the Guangdong Basic and

Applied Basic Research Project (Guangdong Natural Science Foundation) (2019A151511028). The authors thank Haojie Lai and Weiguang Xie of Jinan University, Jinwei Gao and Wei Wei of SCNU, and Qingwu Yin of SCUT for help with AFM, thin film thickness, PL, and TRPL measurements. The authors thank the SCNU Analysis & Testing Center for technical support.

REFERENCES

(1) Li, G.; Zhu, R.; Yang, Y. Polymer Solar Cells. *Nat. Photonics* **2012**, *6*, 153−161.
(2) Yu, G.; Gao, J.; Hummelen, J. C.; Wudl, F.; Heeger, A. J. Polymer Photovoltaic Cells: Enhanced Efficiencies via a Network of Internal Donor-Acceptor Heterojunctions. *Science* **1995**, *270*, 1789−1791.
(3) Duan, C.; Zhang, K.; Zhong, C.; Huang, F.; Cao, Y. Recent Advances in Water/Alcohol-Soluble pi-Conjugated Materials: New Materials and Growing Applications in Solar Cells. *Chem. Soc. Rev.* **2013**, *42*, 9071−9104.
(4) Zhang, G.; Zhao, J.; Chow, P. C. Y.; Jiang, K.; Zhang, J.; Zhu, Z.; Zhang, J.; Huang, F.; Yan, H. Nonfullerene Acceptor Molecules for Bulk Heterojunction Organic Solar Cells. *Chem. Rev.* **2018**, *118*, 3447−3507.
(5) Zhang, Y.; Feng, H.; Meng, L.; Wang, Y.; Chang, M.; Li, S.; Guo, Z.; Li, C.; Zheng, N.; Xie, Z.; Wan, X.; Chen, Y. High Performance Thick-Film Nonfullerene Organic Solar Cells with Efficiency over 10% and Active Layer Thickness of 600 nm. *Adv. Energy Mater.* **2019**, *9*, 1902688.
(6) Fu, H.; Wang, Z.; Sun, Y. Polymer Donors for High-Performance Non-Fullerene Organic Solar Cells. *Angew. Chem., Int. Ed.* **2019**, *58*, 4442−4453.
(7) Cui, C.; Li, Y. High-Performance Conjugated Polymer Donor Materials for Polymer Solar Cells with Narrow-Bandgap Nonfullerene Acceptors. *Energy Environ. Sci.* **2019**, *12*, 3225−3246.
(8) Xu, X.; Feng, K.; Bi, Z.; Ma, W.; Zhang, G.; Peng, Q. Single-Junction Polymer Solar Cells with 16.35% Efficiency Enabled by a Platinum(II) Complexation Strategy. *Adv. Mater.* **2019**, *31*, 1901872.
(9) Gao, K.; Kan, Y.; Chen, X.; Liu, F.; Kan, B.; Nian, L.; Wan, X.; Chen, Y.; Peng, X.; Russell, T. P.; Cao, Y.; Jen, A. K. Y. Low-Bandgap Porphyrins for Highly Efficient Organic Solar Cells: Materials, Morphology, and Applications. *Adv. Mater.* **2020**, *32*, 1906129.
(10) Huang, F.; Bo, Z.; Geng, Y.; Wang, X.; Wang, L.; Ma, Y.; Hou, J.; Hu, W.; Pei, J.; Dong, H.; Wang, S.; Li, Z.; Shuai, Z.; Li, Y.; Cao, Y. Study on Optoelectronic Polymers: An Overview and Outlook. *Acta Polym. Sin.* **2019**, *50*, 988−1046.
(11) Zhao, F.; Wang, C.; Zhan, X. Morphology Control in Organic Solar Cells. *Adv. Energy Mater.* **2018**, *8*, 1703147.
(12) Bartelt, J. A.; Douglas, J. D.; Mateker, W. R.; El Labban, A.; Tassone, C. J.; Toney, M. F.; Frechet, J. M. J.; Beaujuge, P. M.; McGehee, M. D. Controlling Solution-Phase Polymer Aggregation with Molecular Weight and Solvent Additives to Optimize Polymer-Fullerene Bulk Heterojunction Solar Cells. *Adv. Energy Mater.* **2014**, *4*, 1301733.
(13) Huang, F.; Wu, H.; Cao, Y. Water/Alcohol Soluble Conjugated Polymers as Highly Efficient Electron Transporting/Injection Layer in Optoelectronic Devices. *Chem. Soc. Rev.* **2010**, *39*, 2500−2521.
(14) George, Z.; Voroshazi, E.; Lindqvist, C.; Kroon, R.; Zhuang, W.; Wang, E.; Henriksson, P.; Hadipour, A.; Andersson, M. R. Improved Performance and Life Time of Inverted Organic Photovoltaics by Using Polymer Interfacial Materials. *Sol. Energy Mater. Sol. Cells* **2015**, *133*, 99−104.
(15) Fan, B.; Zhang, D.; Li, M.; Zhong, W.; Zeng, Z.; Ying, L.; Huang, F.; Cao, Y. Achieving over 16% Efficiency for Single-Junction Organic Solar Cells. *Sci. China: Chem.* **2019**, *62*, 746−752.
(16) Li, K.; Wu, Y.; Li, X.; Fu, H.; Zhan, C. 17.1%-Efficiency Organic Photovoltaic Cell Enabled with Two Higher-LUMO-Level Acceptor Guests as the Quaternary Strategy. *Sci. China: Chem.* **2020**, *63*, 490−496.
(17) Liu, Q.; Jiang, Y.; Jin, K.; Qin, J.; Xu, J.; Li, W.; Xiong, J.; Liu, J.; Xiao, Z.; Sun, K.; Yang, S.; Zhang, X.; Ding, L. 18% Efficiency Organic Solar Cells. *Sci. Bull.* **2020**, *65*, 272−275.
(18) Zhao, J.; Li, Q.; Liu, S.; Cao, Z.; Jiao, X.; Cai, Y.-P.; Huang, F. Bithieno 3,4-dpyrrole-4,6-dione-Mediated Crystallinity in Large-Bandgap Polymer Donors Directs Charge Transportation and Recombination in Efficient Nonfullerene Polymer Solar Cells. *ACS Energy Lett.* **2020**, *5*, 367−375.
(19) Xu, X.; Xiao, J.; Zhang, G.; Wei, L.; Jiao, X.; Yip, H.-L.; Cao, Y. Interface-Enhanced Organic Solar Cells with Extrapolated T80 Lifetimes of over 20 Years. *Sci. Bull.* **2020**, *65*, 208−216.
(20) Wang, Y.; Zhan, X. Layer-by-Layer Processed Organic Solar Cells. *Adv. Energy Mater.* **2016**, *6*, 1600414.
(21) Huang, Y.; Kramer, E. J.; Heeger, A. J.; Bazan, G. C. Bulk Heterojunction Solar Cells: Morphology and Performance Relationships. *Chem. Rev.* **2014**, *114*, 7006−7043.
(22) Rivnay, J.; Mannsfeld, S. C. B.; Miller, C. E.; Salleo, A.; Toney, M. F. Quantitative Determination of Organic Semiconductor Microstructure from the Molecular to Device Scale. *Chem. Rev.* **2012**, *112*, 5488−5519.
(23) Yan, H.; Ye, S.; Seferos, D. S. Unusual Performance Increase in Polymer Solar Cells by Cooling a Hot Donor/Acceptor Ink in a Good Solvent. *ACS Appl. Mater. Interfaces* **2018**, *10*, 979−984.
(24) Li, Q.; Wang, L.-M.; Liu, S.; Zhan, X.; Zhu, T.; Cao, Z.; Lai, H.; Zhao, J.; Cai, Y.-P.; Xie, W.; Huang, F. Impact of Donor−Acceptor Interaction and Solvent Additive on the Vertical Composition Distribution of Bulk-Heterojunction Polymer Solar Cells. *ACS Appl. Mater. Interfaces* **2019**, *11*, 45979−45990.
(25) Ayzner, A. L.; Doan, S. C.; Tremolet de Villers, B.; Schwartz, B. J. Ultrafast Studies of Exciton Migration and Polaron Formation in Sequentially Solution-Processed Conjugated Polymer/Fullerene Quasi-Bilayer Photovoltaics. *J. Phys. Chem. Lett.* **2012**, *3*, 2281−2287.
(26) Ayzner, A. L.; Tassone, C. J.; Tolbert, S. H.; Schwartz, B. J. Reappraising the Need for Bulk Heterojunctions in Polymer-Fullerene Photovoltaics: The Role of Carrier Transport in All-Solution-Processed P3HT/PCBM Bilayer Solar Cells. *J. Phys. Chem. C* **2009**, *113*, 20050−20060.
(27) Tang, C. W. Two-Layer Organic Photovoltaic Cell. *Appl. Phys. Lett.* **1986**, *48*, 183−185.
(28) Cnops, K.; Rand, B. P.; Cheyns, D.; Verreet, B.; Empl, M. A.; Heremans, P. 8.4% Efficient Fullerene-Free Organic Solar Cells Exploiting Long-Range Exciton Energy Transfer. *Nat. Commun.* **2014**, *5*, 3406.
(29) Markov, D. E.; Amsterdam, E.; Blom, P. W. M.; Sieval, A. B.; Hummelen, J. C. Accurate Measurement of the Exciton Diffusion Length in a Conjugated Polymer Using a Heterostructure with a Side-Chain Cross-Linked Fullerene Layer. *J. Phys. Chem. A* **2005**, *109*, 5266−5274.
(30) Granström, M.; Petritsch, K.; Arias, A. C.; Lux, A.; Andersson, M. R.; Friend, R. H. Laminated Fabrication of Polymeric Photovoltaic Diodes. *Nature* **1998**, *395*, 257−260.
(31) Xu, Y.; Yuan, J.; Liang, S.; Chen, J.-D.; Xia, Y.; Larson, B. W.; Wang, Y.; Su, G. M.; Zhang, Y.; Cui, C.; Wang, M.; Zhao, H.; Ma, W. Simultaneously Improved Efficiency and Stability in All-Polymer Solar Cells by a P−i−N Architecture. *ACS Energy Lett.* **2019**, *4*, 2277−2286.
(32) Dong, S.; Zhang, K.; Xie, B.; Xiao, J.; Yip, H.-L.; Yan, H.; Huang, F.; Cao, Y. High-Performance Large-Area Organic Solar Cells Enabled by Sequential Bilayer Processing via Nonhalogenated Solvents. *Adv. Energy Mater.* **2019**, *9*, 1802832.
(33) Hummelen, J. C.; Knight, B. W.; LePeq, F.; Wudl, F.; Yao, J.; Wilkins, C. L. Preparation and Characterization of Fulleroid and Methanofullerene Derivatives. *J. Org. Chem.* **1995**, *60*, 532−538.
(34) He, Y.; Zhao, G.; Peng, B.; Li, Y. High-Yield Synthesis and Electrochemical and Photovoltaic Properties of Indene-C70 Bisadduct. *Adv. Funct. Mater.* **2010**, *20*, 3383−3389.
(35) Wienk, M. M.; Kroon, J. M.; Verhees, W. J. H.; Knol, J.; Hummelen, J. C.; van Hal, P. A.; Janssen, R. A. J. Efficient

https://dx.doi.org/10.1021/acsenergylett.0c01927
ACS Energy Lett. 2020, 5, 3637−3646

Methano[70]fullerene/MDMO-PPV Bulk Heterojunction Photovoltaic Cells. *Angew. Chem., Int. Ed.* **2003**, *42*, 3371−3375.
(36) Aguirre, J. C.; Hawks, S. A.; Ferreira, A. S.; Yee, P.; Subramaniyan, S.; Jenekhe, S. A.; Tolbert, S. H.; Schwartz, B. J. Sequential Processing for Organic Photovoltaics: Design Rules for Morphology Control by Tailored Semi-Orthogonal Solvent Blends. *Adv. Energy Mater.* **2015**, *5*, 1402020.
(37) Huo, L.; Zhang, S.; Guo, X.; Xu, F.; Li, Y.; Hou, J. Replacing Alkoxy Groups with Alkylthienyl Groups: A Feasible Approach To Improve the Properties of Photovoltaic Polymers. *Angew. Chem., Int. Ed.* **2011**, *50*, 9697−9702.
(38) Zhang, Y.; Li, X.; Dai, T.; Ha, W.; Du, H.; Li, S.; Wang, K.; Meng, F.; Xu, D.; Geng, A. Charge Transport and Extraction of Bilayer Interdiffusion Heterojunction Organic Solar Cells. *J. Phys. Chem. C* **2019**, *123*, 24446−24452.
(39) Rochester, C. W.; Mauger, S. A.; Moulé, A. J. Investigating the Morphology of Polymer/Fullerene Layers Coated Using Orthogonal Solvents. *J. Phys. Chem. C* **2012**, *116*, 7287−7292.
(40) Lee, K. H.; Schwenn, P. E.; Smith, A. R. G.; Cavaye, H.; Shaw, P. E.; James, M.; Krueger, K. B.; Gentle, I. R.; Meredith, P.; Burn, P. L. Morphology of All-Solution-Processed "Bilayer" Organic Solar Cells. *Adv. Mater.* **2011**, *23*, 766−770.
(41) Li, H.; Wang, J. Z. Layer-by-Layer Processed High-Performance Polymer Solar Cells. *Appl. Phys. Lett.* **2012**, *101*, 263901.
(42) Cheng, P.; Hou, J.; Li, Y.; Zhan, X. Layer-by-Layer Solution-Processed Low-Bandgap Polymer-PC61BM Solar Cells with High Efficiency. *Adv. Energy Mater.* **2014**, *4*, 1301349.
(43) Yan, C.; Barlow, S.; Wang, Z.; Yan, H.; Jen, A. K. Y.; Marder, S. R.; Zhan, X. Non-Fullerene Acceptors for Organic Solar Cells. *Nat. Ret. Mater.* **2018**, *3*, 18003.
(44) Zhu, P.; Fan, B. B.; Ying, L.; Huang, F.; Cao, Y. Recent Progress in All-Polymer Solar Cells Based on Wide-Bandgap p-Type Polymers. *Chem. - Asian J.* **2019**, *14*, 3109−3118.
(45) Genene, Z.; Mammo, W.; Wang, E. G.; Andersson, M. R. Recent Advances in n-Type Polymers for All-Polymer Solar Cells. *Adv. Mater.* **2019**, *31*, 1807275.
(46) Zhang, J.; Futscher, M. H.; Lami, V.; Kosasih, F. U.; Cho, C.; Gu, Q.; Sadhanala, A.; Pearson, A. J.; Kan, B.; Divitini, G.; Wan, X.; Credgington, D.; Greenham, N. C.; Chen, Y.; Ducati, C.; Ehrler, B.; Vaynzof, Y.; Friend, R. H.; Bakulin, A. A. Sequentially Deposited versus Conventional Nonfullerene Organic Solar Cells: Interfacial Trap States, Vertical Stratification, and Exciton Dissociation. *Adv. Energy Mater.* **2019**, *9*, 1902145.
(47) Sun, R.; Guo, J.; Sun, C.; Wang, T.; Luo, Z.; Zhang, Z.; Jiao, X.; Tang, W.; Yang, C.; Li, Y.; Min, J. A Universal Layer-by-Layer Solution-Processing Approach for Efficient Non-Fullerene Organic Solar Cells. *Energy Environ. Sci.* **2019**, *12*, 384−395.
(48) Sun, R.; Wu, Q.; Guo, J.; Wang, T.; Wu, Y.; Qiu, B.; Luo, Z.; Yang, W.; Hu, Z.; Guo, J.; Shi, M.; Yang, C.; Huang, F.; Li, Y.; Min, J. A Layer-by-Layer Architecture for Printable Organic Solar Cells Overcoming the Scaling Lag of Module Efficiency. *Joule* **2020**, *4*, 407−419.
(49) McDowell, C.; Abdelsamie, M.; Toney, M. F.; Bazan, G. C. Solvent Additives: Key Morphology-Directing Agents for Solution-Processed Organic Solar Cells. *Adv. Mater.* **2018**, *30*, 1707114.
(50) Wang, L.-M.; Li, Q.; Liu, S.; Cao, Z.; Cai, Y.-P.; Jiao, X.; Lai, H.; Xie, W.; Zhan, X.; Zhu, T. Quantitative Determination of the Vertical Segregation and Molecular Ordering of PBDB-T/ITIC Blend Films with Solvent Additives. *ACS Appl. Mater. Interfaces* **2020**, *12*, 24165−24173.
(51) Sun, Y.; Welch, G. C.; Leong, W. L.; Takacs, C. J.; Bazan, G. C.; Heeger, A. J. Solution-Processed Small-Molecule Solar Cells with 6.7% Efficiency. *Nat. Mater.* **2012**, *11*, 44−48.
(52) Wang, Y.; Zhu, Q.; Naveed, H. B.; Zhao, H.; Zhou, K.; Ma, W. Sequential Blade-Coated Acceptor and Donor Enables Simultaneous Enhancement of Efficiency, Stability, and Mechanical Properties for Organic Solar Cells. *Adv. Energy Mater.* **2020**, *10*, 1903609.
(53) Peet, J.; Cho, N. S.; Lee, S. K.; Bazan, G. C. Transition from Solution to the Solid State in Polymer Solar Cells Cast from Mixed Solvents. *Macromolecules* **2008**, *41*, 8655−8659.
(54) Yuan, J.; Zhang, Y.; Zhou, L.; Zhang, G.; Yip, H.-L.; Lau, T.-K.; Lu, X.; Zhu, C.; Peng, H.; Johnson, P. A.; Leclerc, M.; Cao, Y.; Ulanski, J.; Li, Y.; Zou, Y. Single-Junction Organic Solar Cell with over 15% Efficiency Using Fused-Ring Acceptor with Electron-Deficient Core. *Joule* **2019**, *3*, 1140−1151.
(55) Zhang, J.; Kan, B.; Pearson, A. J.; Parnell, A. J.; Cooper, J. F. K.; Liu, X.-K.; Conaghan, P. J.; Hopper, T. R.; Wu, Y.; Wan, X.; Gao, F.; Greenham, N. C.; Bakulin, A. A.; Chen, Y.; Friend, R. H. Efficient Non-Fullerene Organic Solar Cells Employing Sequentially Deposited Donor−Acceptor Layers. *J. Mater. Chem. A* **2018**, *6*, 18225−18233.
(56) Zhu, T.; Zhan, X.; Xiao, S.; Sun, Y.; Wu, Y.; Zhou, A.; Han, Q. MR: The Multipurpose Reflectometer at CSNS. *Neutron News* **2018**, *29*, 11−13.
(57) Arunagiri, L.; Zhang, G.; Hu, H.; Yao, H.; Zhang, K.; Li, Y.; Chow, P. C. Y.; Ade, H.; Yan, H. Temperature-Dependent Aggregation Donor Polymers Enable Highly Efficient Sequentially Processed Organic Photovoltaics Without the Need of Orthogonal Solvents. *Adv. Funct. Mater.* **2019**, *29*, 1902478.
(58) Kawashima, K.; Fukuhara, T.; Suda, Y.; Suzuki, Y.; Koganezawa, T.; Yoshida, H.; Ohkita, H.; Osaka, I.; Takimiya, K. Implication of Fluorine Atom on Electronic Properties, Ordering Structures, and Photovoltaic Performance in Naphthobisthiadiazole-Based Semiconducting Polymers. *J. Am. Chem. Soc.* **2016**, *138*, 10265−10275.
(59) Ren, M.; Zhang, G.; Chen, Z.; Xiao, J.; Jiao, X.; Zou, Y.; Yip, H.-L.; Cao, Y. High-Performance Ternary Organic Solar Cells with Controllable Morphology via Sequential Layer-by-Layer Deposition. *ACS Appl. Mater. Interfaces* **2020**, *12*, 13077−13086.

https://dx.doi.org/10.1021/acsenergylett.0c01927
ACS Energy Lett. 2020, 5, 3637−3646